

Enhancement of resolution imaging of a flat graded photonic crystal lens using negative refractive index

ABDOLRASOUL GHARAATI^{a,*}, NAJMEH FATHI^a

^a*Department of Physics, Payame Noor University, I. R. of Iran*

The study reported in this article examine the negative refraction of the electromagnetic wave in two-dimensional (2D) triangular lattices graded photonic crystal (GPC) with elliptical cross-section rods (ECSRs). The graded photonic crystal will be obtained by varying the major and minor half axis of the ECSRs in each row. Further, a good quality image, with a relative refractive index of -1, has been observed in this system for transverse electric (TE) polarization. The result suggests that the super-resolution imaging of the point source can be realized by the designed GPC in the second band. Finally, the resolution of the image is compared in different ECSRs elongations and different frequencies in this GPC.

(Received June 2, 2021; accepted November 24, 2021)

Keywords: Graded photonic crystal, Negative effective refractive index, Superlens, Band structures, Equifrequency contours, Finite difference time domain method

1. Introduction

In 1986, negative index materials were predicated with simultaneously negative permittivity and permeability [1-4]. Structures with negative index of refraction form are left-handed set of vectors and called left-hand materials [5-10]. Dielectric photonic crystals (PCs) can also have negative refraction. PCs are periodic dielectric structures with their spatial periodicity on the light wavelength scale [10-21]. In recent years, Centeno et al. examined a type of PC named graded-index (GRIN) [22-23]. Gradual variation of PC parameters, such as the filling factor, radii of the rods, the refractive index, or the lattice constant can be created by graded photonic crystals (GPCs) [24-26]. Generally, it is difficult to describe the propagation behavior of electromagnetic waves in the PC. The well-known method toward the exploration of negative refraction of PC starts from the analysis of the photonic band structures and equifrequency contours (EFCs) [27-28]. Investigating the shape of equifrequency contours can determine the relationship between group velocity v_g and the wave vector k because according to the relation $v_g = \nabla_k \omega(k)$, the wave vector is perpendicular to the equifrequency contours [29-34]. The PC can be considered as homogeneous isotropic medium if the shape of the equifrequency contours is close to a circle [35-36]. On the other hand, the PC with the effective negative index of $n_{eff} = -1$ is similar to the isotropic homogeneous medium with the refractive index of $n = -1$. Recent research studies have indicated that negative refraction can also result from 2D PCs but most of these PCs have circular cross section elements and rarely elliptical elements [30, 33-35], and for elliptical elements, the impact of ellipse changes on imaging resolution has not been studied [30].

The current paper analyzes negative refraction (where the ideal effective index of refraction is $n_{eff} = -1$) on the interface of a 2D hexagonal lattice GPC with ECSR elements. Next, the resolution of imaging is explored by changing the elongation of the elements to design super lens. The plane wave expansion (PWE) method and finite difference time domain (FDTD) method has been applied for the valuable study of the light propagation properties of the band structure and the EFSs in this GPC. Finally, we compare circular cross section with elliptical and by examining the full width at half-maximum at different elongations of the elliptical elements, we show that the elliptical elements cross section has a higher image resolution. And, we show that at the same elongation, the lower frequency of the band has a higher image resolution.

2. Theory of the graded photonic band-gap

For photonic crystals the master equation can be shown as follows:

$$\nabla \times \left(\frac{1}{\epsilon(\vec{r})} \nabla \times \vec{H}(\vec{r}) \right) = \left(\frac{\omega}{c} \right)^2 \vec{H}(\vec{r}) \quad (1)$$

This equation is created by solving Maxwell's equations for the magnetic field [15, 37]. Where $c = 1/\sqrt{\epsilon_0 \mu_0}$ is the speed of light in vacuum, ω is the angular frequency of light and $\epsilon(r) = \epsilon(\vec{r} + \vec{R})$ is position dependent dielectric function which is periodic in terms of the lattice vector \vec{R} [38-39]. For 2D photonic crystals, the band diagrams can be obtained for the two polarizations, namely, transverse electric (TE) polarization and transverse magnetic (TM) polarization. Allowed and

forbidden frequencies can be estimated for a certain wave vector concerning the master equation for all directions. The relation between $\vec{\omega}$ and \vec{k} is called the dispersion relation and defines the band structure of the crystal. Since it defines the group velocity as a gradient of the optical frequency in respect to \vec{k} :

$$v_g = \nabla_k(\omega) \quad (2)$$

Its value is given by the slope of the dispersion curve and its direction is always perpendicular to Iso-frequency contour (IFC). ($\omega(k) = const$) [40].

Consequently, engineering the IFC allows controlling the direction of the wave vector \vec{k} .

Then, we calculate the group index from the slope information of each band of IFC.

The group index can be calculated from the below relation.

$$N_g = \frac{c}{v_g} \quad (3)$$

It is depending on whether \vec{k} is parallel or anti-parallel to group velocity. Many numerical methods can estimate dispersion relations by calculating the master equation. Among them, Finite Difference Time Domain (FDTD) method and the Plane Wave Expansion (PWE) method employed to extract the dispersion properties [41,42].

3. Design and analysis

In the present study, a 2D triangular lattice GPC slab consisting of ECSRs immersed in air with the permittivity equal to ($\epsilon = 12$). The geometry of the GPC is displayed in Fig. 1 (a). Additionally, the GPC is obtained by varying the major and minor half axis of the ECSRs in each row. Let the major and minor radii of the ECSR shown in Fig. 1 (b) be R and r , respectively. It is noteworthy that the values of R and r are identical in each row. The major radius (R) modified from the center of GPC toward the surface as 0.45, 0.42, 0.38, 0.35 and the elongation of ECSRs in the GPC structure is equal to 1.1, ($e = r/R = 1.1$)

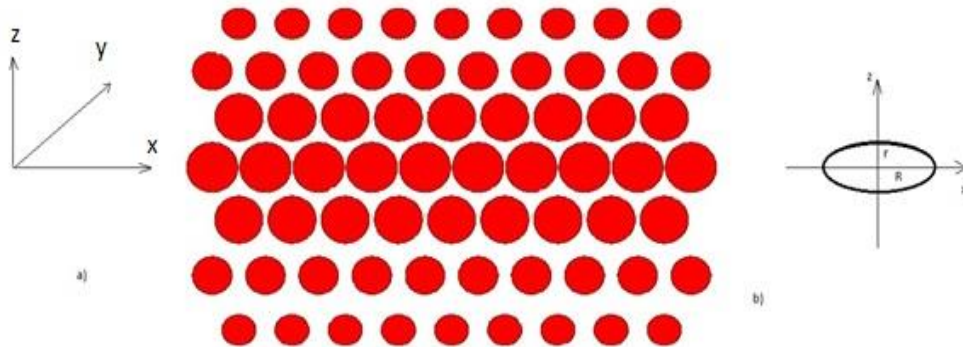


Fig. 1. (a) A schematic of the GPC with ECSRs that in X-Z plane, (b) schematic elongation of elliptical ($e = r/R$) that created by the major(R) and minor(r) radii

The plane-wave expansion method has been used to determine the band structures and EFCs. Fig. 2 depicts the band structure of 2D GPC of hexagonal lattice for the transverse electric (TE) polarization and the light line shifted to point is shown in green.

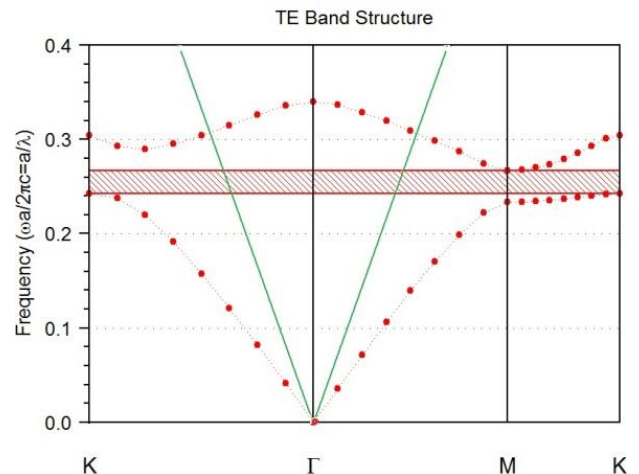


Fig. 2. Band structures of 2D GPC made of ECSRs ($\epsilon = 12$) arranged a hexagonal lattice embedded in vacuum (color online)

The group velocity of the transmitted electromagnetic waves can be calculated from the EFCs. The TE polarized EFCs of the second band of GPC have been plotted in Fig. 3. Apparently, the directions of the wave vector and group velocity are opposite, this implies that the effective index is negative. Since the EFCs are almost circular, the GPC structure can be regarded as a homogeneous medium. Thereby, the effective index n_{eff} can be obtained from the ratio of the EFC radius to the relation of dispersion of the vacuum, which is generally called the light cone [36].

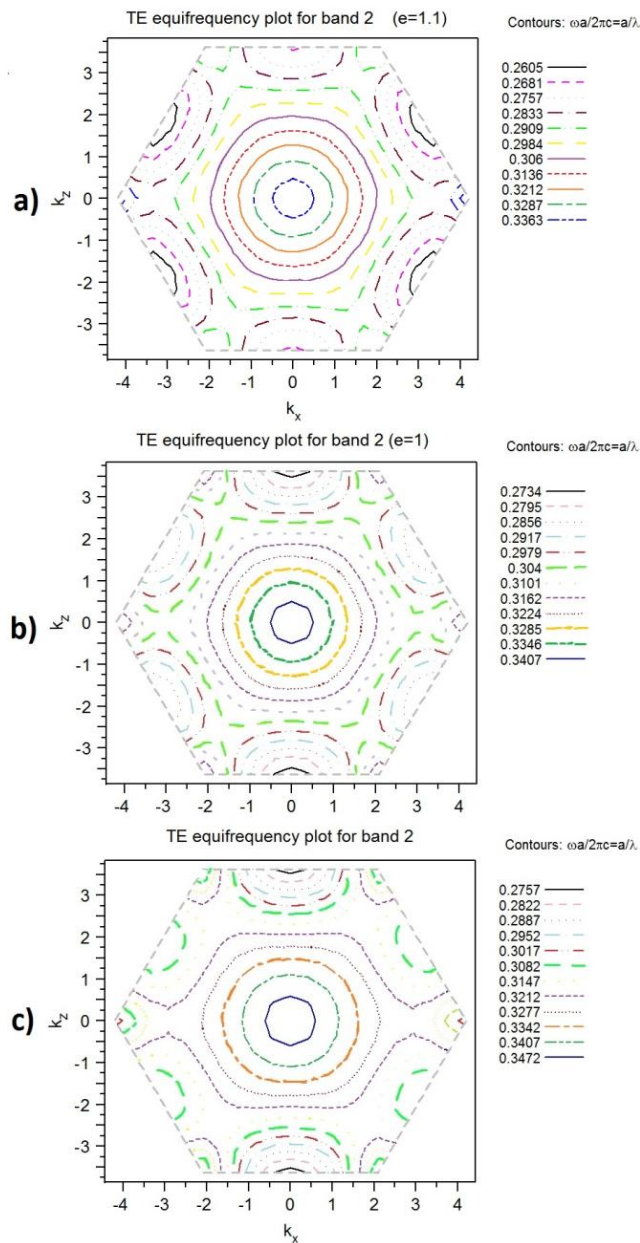


Fig. 3. The TE polarized EFCs of the second band of GPC, frequency values are in units of $(2\pi c/a)$ (a) $e=1.1$, (b) $e=1$, (c) $e=0.9$ (color online)

As can be inferred From Figs. 2 and 3, the frequency $\omega = 0.306(2\pi c/a)$, the radius of GPC contour is equal to the radius of the air contour and so the effective negative index is $n_{eff} = -1$.

On the other hand, according to equation (3), the effective refractive index diagram for the second TE band shows in Fig. 4. It can be deduced that when frequency is higher than $\omega = 0.306(2\pi c/a)$, $n_{eff} > -1$ for frequency lower than $\omega = 0.306(2\pi c/a)$, $n_{eff} < -1$.

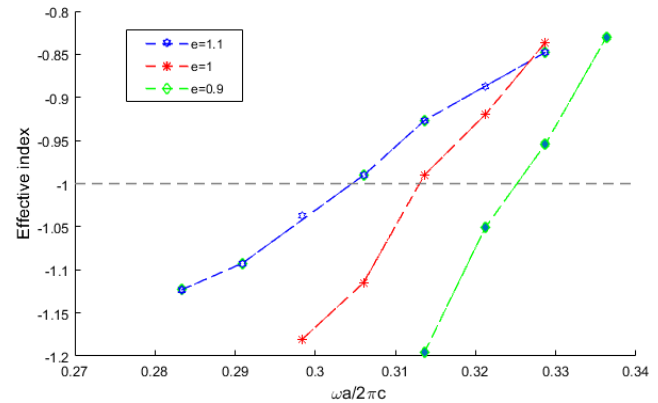


Fig. 4. Effective indexes vs. frequencies for TE polarization, the position of relative refractive index of -1 is marked by the dotted line (color online)

In the next chapter, we will focus on the negative refractive index of -1 to demonstrate that the superlens effect occurs in this GPC slab system.

4. Negative refraction and superlens effect in the designed GPC

It is obvious from the EFC contours (Fig. 3) that the group velocities (v_g) are opposite to the phase velocity. This is evidence that the transmitting feature of the wave in the second band of GPC structure has the left-hand behavior. Fig. 5 reveals the electric field intensities of the Gaussian beam passing through the GPC. The outgoing beam has the same propagation direction as the incoming beam but with a negative transverse shift. We have used the GPC with a negative refraction index in which has included 7 rows in the Z direction and 40 columns in the X-direction. In our calculations, the width of the sample is large enough to prevent the effects of edge diffraction.

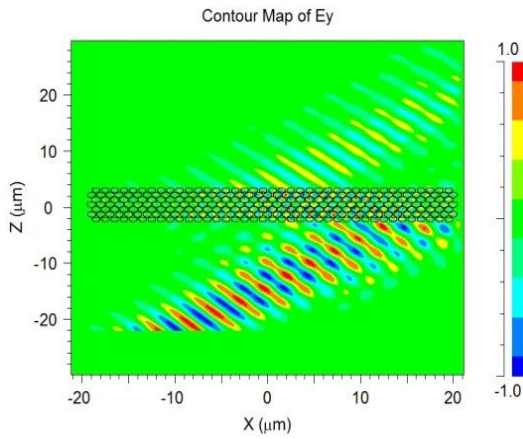


Fig. 5. Simulation of negative refraction. The frequency of the incident electromagnetic wave beam is $\omega = 0.306(2\pi c/a)$ (color online)

The most important and significant application of GPC with the effective refractive index of -1 is perfect superlens imaging [42-44]. A superlens can fixate a point source on one dimension of the lens into a real point image on the other dimension. In order to show the designed GPC as a superlens in the previous chapter, the finite difference time domain (FDTD) method employed, incorporating the perfectly matched layer (PML) boundary conditions to visualize the propagation of the TE polarized electromagnetic wave through the proposed GPC structure [45]. In this regard, a continuous wave point source with $\omega = 0.306(2\pi c/a)$ frequency has been put, which is corresponded to the case with the relative refractive index of -1. Many recent works of GPC imaging have revealed that the sum of source distance and image distance is equal to the thickness of the GPC slab. Then, the thickness of the PC slab should be chosen carefully to maximize transmission for all incident angles [46-47]. The high-quality image occurs when the source distance from the center of the slab is equal to the thickness of the slab (d) and should observe the image at the symmetric position on the opposite side of the slab. (Fig. 6) The distance between source and image is 2d, where d is the thickness of the slab, [41]. Thus, if the point source is closer to the GPC, its image will be farther away and conversely.

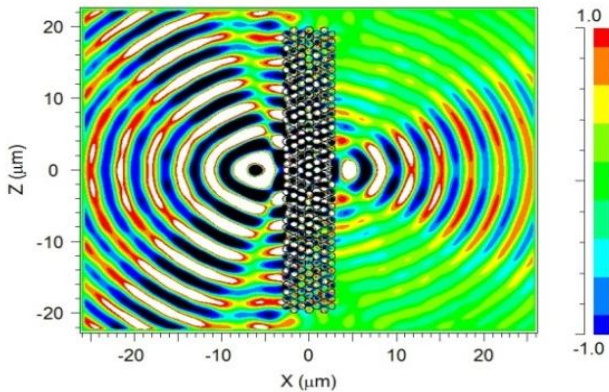


Fig. 6. The electric field distribution of the point source and its image across the GPC flat lens at the frequency $\omega = 0.306(2\pi c/a)$ for the TE wave (color online)

5. Comparison of image resolution in the designed GPC at different elongation

One of the most important image quality parameters is image resolution. There are several criteria for evaluating image quality. Many authors have employed the Full-Width Half Maximum (FWHM) to measure the image resolution because it is easy to get the FWHM of the image intensity [42,48]. Hence, we use the FWHM to analyze the image with designed GPC to explore this issue, the electric field intensity distributions across the image plane for the GPC with $e = 1.1$, $e = 1$ and $e = 0.9$ are shown in Fig. 7 and Fig. 8. A continuous-wave point source with frequency $\omega = 0.306(2\pi c/a)$ is placed at a distance $0.6a$, from the left surface of the GPC slab. As shown in Fig. 7, the FWHM for $e = 1.1$ is about $\Delta = 0.471\lambda$, and it increases for $e = 1$, ($\Delta = 0.50\lambda$) and $e = 0.9$, ($\Delta = 0.527$). Consequently, the spatial resolution of the designed GPC slab with $e = 1.1$ is better than that of the GPC slab with $e = 1$ and $e = 0.9$.

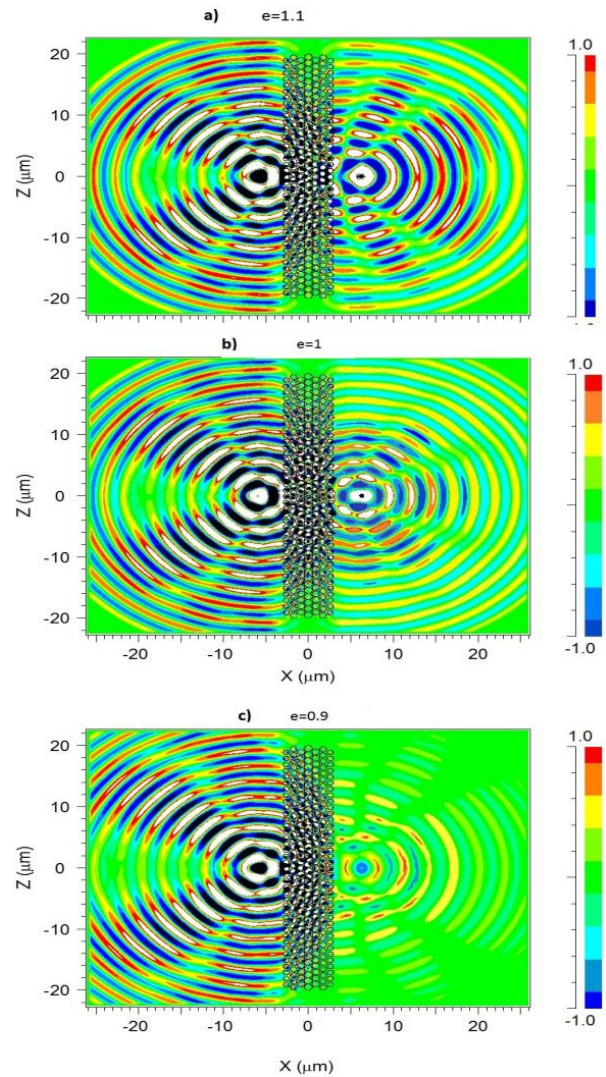


Fig. 7. The field distribution for different elongations of structure, the elongation is equal to $e = 1.1, e = 1, e = 0.9$ in (a), (b) and (c), respectively (color online)

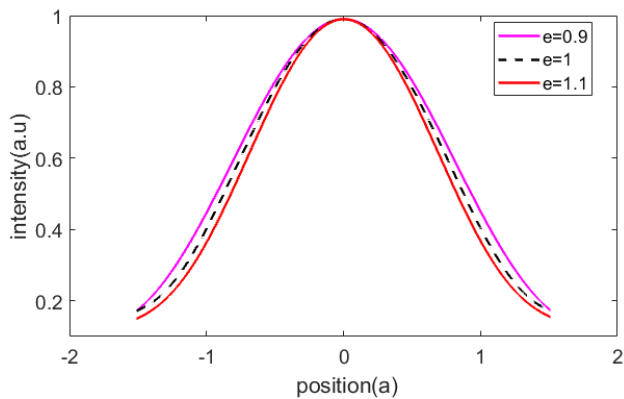


Fig. 8. The distribution of the electric field intensity at the image place for different elongations (color online)

6. Comparison of image resolution at different frequencies in the designed GPC

In this chapter, the image resolution has been analyzed by changing frequencies in the designed GPC with $e = 1.1$.

The FWHM for this GPC has been calculated, in which frequencies $\omega = 0.301(2\pi c/a)$, $\omega = 0.306(2\pi c/a)$, $\omega = 0.309(2\pi c/a)$. The FWHM values calculate for the three frequencies are respectively equal to $\Delta = 0.447\lambda$, $\Delta = 0.471\lambda$ and $\Delta = 0.496\lambda$.

The frequency $\omega = 0.301(2\pi c/a)$ reveals the lowest FWHM, which indicates a higher image resolution (Fig. 9).

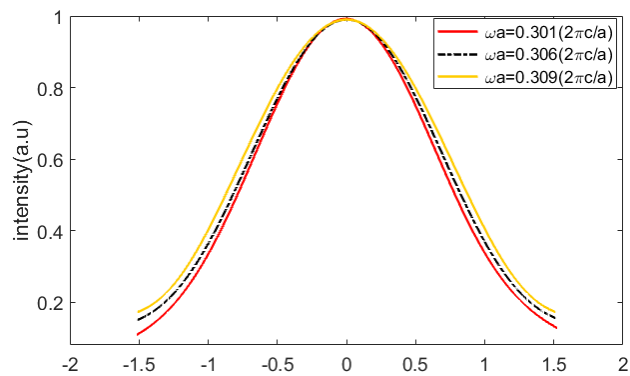


Fig. 9. The distribution of the electric field intensity at the image place for different frequencies (color online)

7. Conclusions

Based on the band structure analysis, we examined left-hand behavior in a 2D triangular lattice photonic crystal slab consisting of ECSRs immersed in air. Furthermore, we have also shown the relative refractive index of -1 for Gaussian beam incidence. In this system, an image with a remarkable quality was observed. These

features are close to the ideal system that can serve as a perfect superlens. Then, we studied the resolution of the image by changing the elongation of the elements. The analysis of the FWHM resolution indicated that for $e = 1.1$ the imaging quality is better than the other elongations. This structure 5.8 % is better than circular ones. And at the same elongation, the GPC with frequency $\omega = 0.301(2\pi c/a)$ had a higher image resolution. It is shown that this frequency 10.6% is better than the others.

References

- [1] V. G. Veselago, Soviet Physics Uspekhi **10**, 509 (1968).
- [2] P. Markos, C. M. Soukoulis, Physical Review B **65**, 3 (2001).
- [3] A. Sukhovanov, V. Guryev, Photonic Crystals: Physics and Practical Modeling, Springer Series in Optical Science (New York, 2009).
- [4] A. Houwe, Mustafa Inc, S. Y. Doka, M. A. Akinlar, D. Baleanu, Results in Physics **17**, 103097 (2020).
- [5] R. Gajic, R. Meisels, F. Kuchar, K. Hingerl, Optics Express **13**, 8596 (2005).
- [6] M. Rajput, R. K. Sinha, International Conference on Optics and Photonics **7420**, 1 (2009).
- [7] S. Rafiee Dastjerdi, M. Ghanaatshoar, K. Delfanazari, International Journal of Optics and Photonics **8**, 41 (2014).
- [8] S. A. El-Naggar, Eur. Phys. J. D **71**, 11 (2017).
- [9] F. Xi, L. Hu, Eur. Phys. J. D **67**, 224 (2013).
- [10] F. Xi, L. Hu, Eur. Phys. J. D **66**, 33 (2012).
- [11] Z. Zare, A. Gharaati, Eur. Phys. J. D **74**, 140 (2020).
- [12] Z. Dorrani, Journal of Optoelectronic Nanostructures **24**, 2675 (2007).
- [13] R. Kun, R. Xiaobin, Science China Press and Springer-Verlag Berlin Heidelberg **57**, 1241 (2012).
- [14] J. Joannopoulos, S. Johnson, J. Winn, R. Meade, Photonic Crystals: Modeling the Flow of Light Princeton University Press, Princeton, 2008.
- [15] K. Sakoda, Optical Properties of Photonic Crystals, 2nd ed. (Springer-Verlag, New York, 2004).
- [16] B. Saleh, M. Teich, Fundamental of Photonics, 2 Volume Set, 3rd Edition, Wiley, New York, 2019.
- [17] C. Sibilia, T. Benson, M. Marciniak, T. Szoplík, Photonic Crystals: Physics and Technology, Springer-Verlag Italia, 2008.
- [18] M. Skrobogatiy, J. Yang, Fundamental of Photonic Crystal Guiding **51**, 177 (2010).
- [19] Z. Zare, A. Gharaati, Physica B **553**, 105 (2019).
- [20] H. Azarshab, A. Gharaati, Microelectronic Engineering **198**, 93 (2018).
- [21] H. Azarshab, A. Gharaati, J. Optoelectron. Adv. M. **13**(20-25), 2 (2019).
- [22] E. Centeno, D. Cassagne, Optics Letters **30**, 2278 (2005).
- [23] H. Kurt, D. S. Citrin, Optics Express **15**, 1240 (2007).

- [24] M. Turdjev, I. H. Giden, H. Kurt, *Optics Communications* **339**, 22 (2015).
- [25] A. Gharaati, N. Miri, Z. Zareian, *Journal of Optoelectronic Nanostructures* **2**, 49 (2017).
- [26] M. Notomi, *Physical Review B* **62**, 10696 (2000).
- [27] J. B. Pendry, *Physics Review Letters* **85**, 3966 (2000).
- [28] C. Luo, S. G. Johnson, J. D. Joannopoulos, J. B. Pendry, *Physics Review B* **68**, 1 (2003).
- [29] J. Xie, J. Wang, R. Ge, B. Yan, E. Liu, W. Tan, *Journal of Physics D Applied Physics* **51**, 205103 (2018).
- [30] F. Shuai, A. Ling, W. Yi-Quan, L. Zhi-Yung, Z. Dao-Zhong, *Chinese Physics Letters* **24**, 2675 (2007).
- [31] F. Gauffillet, E. Akmansoy, *Journal of Applied Physics* **114**, 083105 (2013).
- [32] F. Gauffillet, E. Akmansoy, *IEEE Photonics Journal* **8**, 2400211 (2016).
- [33] M. L. Liu, M. J. Yun, F. Xia, W. J. Kong, Y. Wan, J. Liang, W. Lv, H. Y. Tan, *Progress in Electromagnetics Research M* **25**, 185 (2012).
- [34] W. Li, Z. He, K. Deng, H. Zhao, *Results in Physics* **6**, 165 (2016).
- [35] X. Zhang, *Physics Review B* **70**, 195110 (2004).
- [36] P. Jiang, K. Xie, H. Yang, Z. Wu, *International Journal of Photoenergy* **2012**, 1 (2011).
- [37] F. Segovia-Chavesa, H. Vinck-Posada, *Results in Physics* **16**, 102947 (2020).
- [38] Y. Kalra, R. K. Shinha, *Journal of Physics* **67**, 1155 (2006).
- [39] O. Hess, C. Hermann, A. Klaedtke, *Physica Status Solidi* **197**, 605 (2003).
- [40] A. Gharaati, N. Miri, *Ukr. J. Phys. Opt.* **18**(2), 109 (2017).
- [41] C. Lou, S. G. Johnson, J. D. Joannopoulos, J. B. Pendry, *Physics Review B* **65**, 201104 (2002).
- [42] A. Gharaati, N. Miri, *J. Optoelectron. Adv. M.* **11**(608-615), 12 (2017).
- [43] H. Kurt, E. Colak, O. Cakmak, H. Caglayan, E. Ozbay, *Applied Physics Letters* **104**, 031116 (2008).
- [44] L. Jiang, H. Wu, W. Jia, X. Li, *Journal of Applied Physics* **111**, 023508 (2012).
- [45] X. Wang, Z. F. Ren, K. Kemoa, *Optics Express* **12**, 2919 (2004).
- [46] G. Sun, A. S. Jugessur, A. G. Kirk, *Optics Express* **15**, 6755 (2006).
- [47] N. Miri, A. Gharaati, *Journal of Optoelectronic Nanostructures* **2**(2), 55 (2017).
- [48] S. Castiñeira-Ibáñez, D. Tarrazó-Serrano, P. Candelas, O. V. Minin, C. Rubio, I. V. Minin, *Results in Physics* **15**, 102582 (2019).

*Corresponding author: agharaati@pnu.ac.ir